RSC Advances

PAPER

View Article Online
View Journal | View Issue

Cite this: *RSC Adv.*, 2019, **9**, 29796

Electrochemical degradation of ciprofloxacin with a Sb-doped SnO_2 electrode: performance, influencing factors and degradation pathways†

Yanguang Mu,[a] Cong Huang,[a] Haipu Li,*[ab] Leilei Chen,[a] Ding Zhang[a] and Zhaoguang Yang*[ab]

Sb-doped SnO_2 electrodes were prepared with the practical sol–gel method and were used for the electrocatalytic degradation of ciprofloxacin (CIP) in aqueous solution. Results from the electrochemical characterization (including cyclic voltammetry, linear sweep voltammetry, and electrochemical impedance spectroscopy) showed that the electrode with 16 coating times (SSO-16) had the highest oxygen evolution potential of 2.2 V (*vs.* SCE) and the highest electrochemically active area of 3.74 cm^2. The results of scanning electron microscopy and X-ray diffraction showed that the coating times could affect the surface morphology and crystal structure of the electrodes, and the SSO-16 electrode had a denser surface, higher crystallinity, and smaller grain size (28.6 nm). Moreover, the experimental parameters for CIP degradation with SSO-16 were optimized, and the removal ratio of CIP reached to almost 100% within 60 min. In addition, the possible degradation pathways of CIP were proposed. And the stability and reusability of the SSO-16 electrode were also studied. These results are valuable for the preparation of high electrocatalytic performance electrodes by a sol–gel coating method for electrochemical degradation of antibiotics.

Received 27th June 2019
Accepted 4th September 2019

DOI: 10.1039/c9ra04860j

rsc.li/rsc-advances

1. Introduction

In recent years, increasing amounts of antibiotics have been produced and consumed. In 2011, the estimated consumption of antibiotics was 89 700 tons in China, while it had doubled in 2016.[1,2] Meanwhile, antibiotics have been frequently detected in surface water,[3] effluent and excess sludge of municipal wastewater treatment plants,[4,5] and even ground water.[6–8] The traditional wastewater treatment technology cannot completely remove these antibiotics, because the physical process can not degrade the contaminants and the biological treatment process will be restricted by the antibacterial properties of the antibiotics.[9,10] Considering the potential threat of antibiotic residues to the global environment and human health, the effective degradation of antibiotics is becoming a matter of concern for environmental protection.

Advanced oxidation processes, including Fenton oxidation, electrochemical oxidation and photocatalysis, have always been praised as viable methods on wastewater treatment.[11–16] By comparison, electrochemical oxidation has great advantages in the treatment of refractory organic wastewater because of its high processing efficiency, simple equipment, convenient operation, and environmental friendliness.[17] The anode materials are vital for electrochemical oxidation because they determine the formation of hydroxyl radicals.[18] The electrode materials, including SnO_2,[19] PbO_2,[20] and boron doped diamond,[21] had been widely used in wastewater treatment. Among them, the Sb-doped SnO_2 electrode has a wonderful application prospect due to its excellent electrochemical activity, chemical stability, and electrical conductivity.[22] Currently, the common preparation methods include sol–gel coating method,[23–25] electrodeposition,[26,27] spray pyrolysis,[28] and hydrothermal synthesis.[29] Since the sol–gel coating method is simple in operation and easy to mass produce, the Sb-doped SnO_2 electrode is usually prepared by this method.[25] About the sol–gel method, the influences of the doping amount of Sb element and calcination temperature on the performance of the electrode had been studied.[22,30,31] The results showed that the electrode would possess good catalytic activity when the doping amount of Sb was 6–9% and the calcination temperature was 550 °C. However, little research has investigated the electrocatalytic degradation efficiency of the electrodes prepared with different numbers of coating operations.

As an effective broad-spectrum antibiotic of the third generation fluoroquinolones, ciprofloxacin (CIP) has strong antibacterial activity against many bacteria, such as *Escherichia*

[a]*Center for Environment and Water Resources, College of Chemistry and Chemical Engineering, Central South University, Changsha 410083, PR China. E-mail: lihaipu@csu.edu.cn; zgyang@csu.edu.cn*

[b]*Key Laboratory of Hunan Province for Water Environment and Agriculture Product Safety, Changsha 410083, PR China*

† Electronic supplementary information (ESI) available. See DOI: 10.1039/c9ra04860j

coli, *Pseudomonas aeruginosa*, and *Staphylococcus aureus*. However, it is quite stable in the environment. Herein, CIP was selected as the target to evaluate the electrocatalytic activities of the investigated Sb-doped SnO_2 electrodes, which were fabricated by the sol–gel method with different coating times. In order to understand the effects of the coating times on the structure and composition of the electrodes, the electrodes were characterized by scanning electron microscopy (SEM) and X-ray diffraction (XRD). And the electrochemical properties of these electrodes were also investigated by cyclic voltammetry (CV), linear sweep voltammetry (LSV), and electrochemical impedance spectroscopy (EIS). Moreover, the effects of current density, electrolyte concentration, initial concentration and initial pH of the substrate solutions on the removal of CIP were also explored so that it could provide valuable information for the removal of CIP in practical applications. Meanwhile, the possible intermediates formed in the degradation process were analyzed by HPLC-MS/MS, and the possible degradation pathways were proposed. Finally, the reusability of the Sb-doped SnO_2 electrode was also studied.

2. Experimental

2.1. Materials and instruments

The chemicals and reagents were all analytical grade. $SnCl_4 \cdot 5H_2O$, $SbCl_3$, and CIP (>98%) were provided by Aladdin Reagent Co. Ltd. (Shanghai, China). Others were purchased from Sinopharm Group Co. Ltd. (Beijing, China). The titanium plates were obtained from Bojie Co. Ltd. (Baoji, China). Ultrapure water (18.25 MΩ cm) for all the solutions was produced using an Ultrapure Water Purification System from Ulupure Corporation (Sichuan, China). All reagents were used directly without further purification.

2.2. Electrode preparation

Titanium plate (20 mm × 20 mm × 1 mm) was polished with sandpaper (1200 mesh) and degreased at 90 °C for 1 hour in 10 wt% NaOH solution. Then, it was etched at 90 °C for 2 hours in 10% boiling oxalic acid solution and finally rinsed with deionized water.[25]

The electrode was prepared by a sol–gel method.[32] Citric acid was mixed with ethylene glycol at 70 °C, and then the solution was heated to 90 °C. $SnCl_4 \cdot 5H_2O$ and $SbCl_3$ were added to the solution in a molar ratio of citric acid : ethylene glycol : $SnCl_4 \cdot 5H_2O$: $SbCl_3$ of 130 : 30 : 9 : 1. The sol–gel was obtained by holding the solution at 90 °C for 30 min. Then, the sol–gel was applied to coat the prepared titanium plate. Finally, the coated titanium plate was baked in an infrared oven and then sintered for the thermal deposition at 550 °C in a muffle furnace for 10 min. After cooling to room temperature, the above coating-bake-thermal deposition process was repeated several times, and the titanium plate was annealed at 550 °C for 2 hours in the last time. The obtained electrodes were named as SSO-8, SSO-10, SSO-12, SSO-14, SSO-16, and SSO-20, where the numbers represented the times of coating operations.

2.3. Characterization of electrodes

The surface and composition of electrodes were characterized by SEM (Zeiss Sigma HD, Germany) and XRD (Bruker D8 Advance, Germany) with Cu (Kα) radiation at 40 kV/40 mA.

The electrochemical performance of as-prepared electrode was evaluated in a three-electrode system at room temperature on CHI604E electrochemical workstation (Shanghai, Chenhua Instrument Co. Ltd., China) with saturated calomel electrode (SCE) as the reference electrode, platinum sheet as the counter electrode. The potentials appearing in the text were referred to SCE. Electrochemical double-layer capacitance was measured using CV in 0.5 M KOH solution, and the potential scanning range was from 0.5 V to 0.6 V. The CV was also used to test the electrochemical active area of the electrode in 0.1 M KCl and 1 mM $K_3Fe(CN)_6$ solution by sweeping from −0.1 V to 0.5 V. The LSV curves were tested in 0.5 M H_2SO_4 solution with a sweep rate of 50 mV s^{-1}. The EIS was carried out in the AC frequency range of 100 000–0.1 Hz with the amplitude of 5 mV under the applied potential of 2 V and the results were fitted using Zsimpwin software.

2.4. Detection of hydroxyl radical

The terephthalic acid fluorescence method was used to detect the hydroxyl radical.[33] The tests were performed in a solution (100 mL) containing 0.5 mM terephthalic acid, 2.0 mM NaOH, and 0.25 M Na_2SO_4. The as-prepared electrodes and a stainless steel plate were used as anode and cathode, respectively. The applied current density was 15 mA cm^{-2}. During the tests, 2 mL solutions were taken every 5 min for fluorescence spectroscopy. The produced 2-hydroxy terephthalic acid was measured by a fluorescence spectrometer (Hitachi F-7000, Japan) with the excitation wavelength of 315 nm and emission wavelength of 425 nm.

2.5. Electrochemical degradation experiment

The CIP solution (50 mL) was degraded in a quartz beaker with Na_2SO_4 as the supporting electrolyte under a galvanostatic condition. The as-prepared SSO electrodes and a stainless steel plate were used as anode and cathode, respectively, with a submerged geometric surface area of 4 cm^2. The distance between the two electrodes was 3 cm. Effects of coating times (8–20), current density (10–25 mA cm^{-2}), electrolyte concentration (10–40 g L^{-1}), initial concentration (10–80 mg L^{-1}), and pH value (3–9) on degradation were investigated. During experiments, samples were taken every 15 min, and UV–vis Spectrophotometer (TU-1901, Beijing, China) was mainly used to monitor the removal rate of CIP in terms of variances in the absorbance, and the main absorption peak (λ_{max}) located at 275 nm.[34,35] The removal rate was calculated as follows: removal rate of CIP = $(C_0 - C_t)/C_0 \times 100$, where C_0 and C_t were the concentration of CIP at the initial and sampling time, respectively.

Furthermore, the three-dimensional excitation-emission matrix fluorescence spectra (3D EEM) and HPLC-MS/MS were also used to assist the monitoring of the degradation. The 3D

EMM were recorded using an Aqualog UV 800 (HORIBA Instruments Incorporated, USA). The final concentration of CIP and possible intermediates during the degradation progress were monitored by an Agilent 6460 triple quadrupole mass spectrometer equipped with an electrospray ionization source, combined with an Agilent 1260 series Liquid Chromatography system (HPLC-MS/MS) (Agilent, Palo Alto, CA, USA). The details were provided in the ESI (Text S1).†

3. Results and discussion

3.1. Characterization of the electrode structure

3.1.1. SEM images. The surface morphologies of the electrodes with different coating times recorded by SEM were shown in Fig. 1. It could be seen that there are significant differences in the morphologies of the electrodes prepared with different coating times. Among them, the surface morphologies of the SSO-12, SSO-14, and SSO-16 were more compact. Larger holes were observed on the surface of the SSO-8, SSO-10, and SSO-20. It may be attributed to the low coating times for the former two electrodes and the excessive coating and frequent calcination for the latter electrode. As illustrated in Fig. 1e, the surfaces of the SSO-16 had more regular and compact nanoparticles with the size in a range of 50–200 nm, which would increase electrode stability and extend electrode life through preventing inner Ti plates from being corroded by the electrolytes,[36] and enlarge the specific surface area of the electrodes, provide more active centers and thus enhance the electrochemical oxidation activity of the electrode as well.[37] These were different from the previously reported cracked coating.[19,30]

3.1.2. XRD. Fig. 2 shows the XRD patterns of the Sb-doped SnO_2 electrodes, which provides information about phase structure and the composition of as-prepared electrodes. There were stronger peaks at the 2θ values of 25.6°, 33.9°, and 51.8°, which corresponded to the (110), (101), and (211) crystal planes of rutile phase SnO_2 (JCPDS no. 72–1147), respectively; indicating that the rutile phase SnO_2 might be obtained on the surface of electrodes. It was also noticed that the peak of SSO-8 at 25.6° was very weak and two strong Ti diffraction peaks (40.1° and 70.9°) were also detected, which might be attributed to the low coating times and poor crystallinity. As increasing the coating times, the relative peak intensities of SnO_2 increased gradually. Meanwhile, those peaks of Ti and TiO_2 decreased rapidly.

The crystal sizes estimated by the Scherer formula and the lattice parameters calculated using Bragg's equation were listed in Table S1.† It could be seen that the crystal size of the SSO-12 (12.2 nm) was the smallest, while those of SSO-14 and SSO-16 were 14.8 and 28.6 nm, respectively. Compared with the lattice parameters of SnO_2 (JCPDF 72-1147), these calculated values of the prepared electrodes all decreased. This may be due to that the radius of doped Sb^{5+} ion was smaller than that of Sn^{4+} ion.[22]

3.2. Electrochemical characterization

3.2.1. Electrochemical active surface area. The electrochemical active surface areas of these electrodes were explored in $K_3Fe(CN)_6$ solution by CV. It could be seen from the Fig. S1†

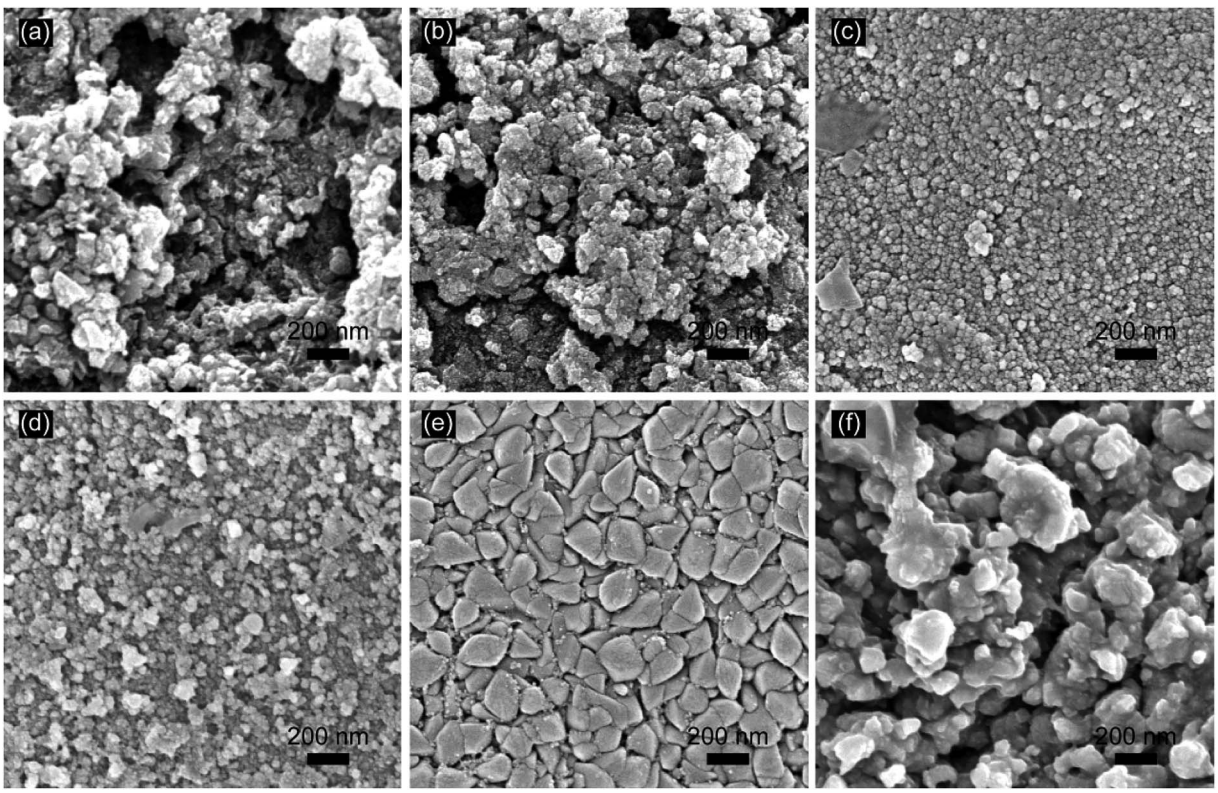

Fig. 1 SEM images of the prepared electrodes: (a) SSO-8, (b) SSO-10, (c) SSO-12, (d) SSO-14, (e) SSO-16, (f) SSO-20.

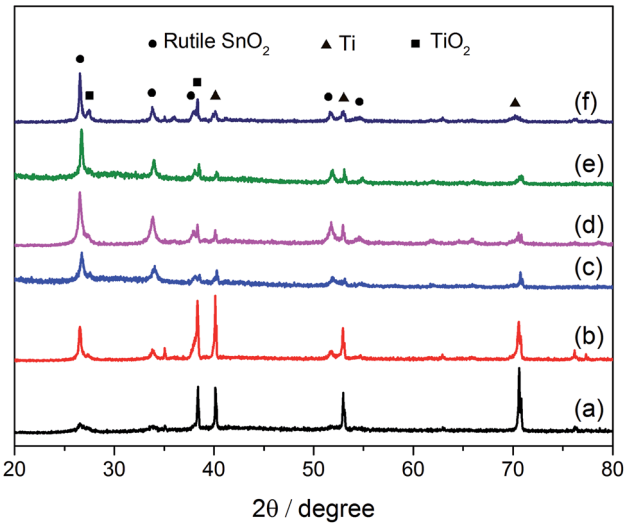

Fig. 2 XRD patterns of the prepared electrodes: (a) SSO-8, (b) SSO-10, (c) SSO-12, (d) SSO-14, (e) SSO-16, (f) SSO-20.

that each electrode had a pair of redox peaks corresponding to the reaction between $K_3Fe(CN)_6$ and $K_4Fe(CN)_6$ in the potential range of 0.5 V to −0.1 V. Fig. 3a shows the cathode peak current of the CV curves with the different electrodes.

Obviously, the SSO-16 had the largest i_{pc}, indicating that the $Fe(CN)_6^{3-}$ on the electrode surface could be converted to $Fe(CN)_6^{4-}$ more quickly. Electrochemical active surface areas were calculated using Randles–Sevcik equation:

$$i_{pc} = 268600n^{1.5}CD^{0.5}Av^{0.5} \quad (1)$$

where i_{pc} is the cathode peak current of the CV curves, n is the number of transferred electrons (1 mol), C is the bulk concentration of $K_3Fe(CN)_6$ (10^{-6} mol cm^{-3}), D is the diffusion coefficient of $K_3Fe(CN)_6$ in 0.1 M KCl solution (6.3×10^{-6} cm^2 s^{-1}), A is the electrochemical active surface area of the electrodes (cm^2), and v is the scan rate (V s^{-1}). The values of A, obtained from the slope of i_{pc} *vs.* $v^{0.5}$, were shown in Table S1.† Although each electrode had a same geometric area of 4 cm^2, the SSO-16 had an electrochemical active area of 3.74 cm^2, higher than others.

3.2.2. LSV curves. The oxygen evolution potential (OEP) is a supreme parameter for evaluating electrode performance.[35] Sb–SnO_2 has a high OEP, which is considered to be one of the most promising wastewater treatment electrode material.[38] Fig. 3b shows the LSV curves of the prepared electrodes measured in 0.5 M H_2SO_4 solution at a scan rate of 50 mV s^{-1}. The current density of the SSO-8 was very small at 2.5 V because the coating times were low and the resistance of the electrode was very large. And the SSO-16 had the highest OEP of 2.2 V implying that a large number of hydroxyl radicals could be released to remove organic pollutants.[39]

3.2.3. Electrochemical double layer capacitance. The electrochemical double layer capacitance (C_{dl}) was measured by CV. As could be seen in Fig. S2,† there was not redox peak corresponding to the electrochemical reaction. The difference between the forward sweep current and the reverse sweep current at 0.55 V was regarded as the capacitor current (I_{dl})[40] (shown in Fig. 3c). The values of C_{dl} obtained from the slopes of the I_{dl} *vs.* v plots were shown in Table S1.† The C_{dl} values of the SSO-12 and SSO-16 were 7.07 mF and 5.83 mF, respectively, implying the larger specific surface areas which were more conducive to the degradation of organics.[41]

3.2.4. Electrochemical impedance spectroscopy (EIS). The Nyquist plots of all as-prepared electrodes were quite similar (shown in Fig. 3d). The same equivalent circuit model shown in Fig. 3e was used to simulate the EIS data and the fitting results were shown in Table S2.† The R_e in the model represents the electrolyte resistance. Parallel capacitors and resistors ($R_{ads}\|C_{ads}$) are used to describe the adsorption and desorption process of hydroxyl radicals.[42] The R_{ct} describing the charge transfer at the electrode/electrolyte interface determined the electrocatalytic activity of the electrode. The semicircle in the low frequency range corresponds to the electrochemical double layer capacitor represented by a constant phase element.[27] The R_{ct} value of the SSO-8 was 865.70 Ω cm^2, while those of the SSO-12 and SSO-16 were 5.97 and 8.46 Ω cm^2, respectively, suggesting that the coating times had a significant impact on the interface charge transfer. Moreover, the R_{ct} was much smaller than the R_{ads}, indicating that the controlling step of the surface discharge process was the adsorption/desorption process.[43]

3.3. Electrochemical degradation of CIP

3.3.1. Effect of coating times. The electrodes with different coating times were used as the anode, and the stainless steel plate was used as the cathode. The results in Fig. 3f shows that the removal rate of CIP depended on the coating times. When the coating times increased from 8 to 16, the removal rates increased gradually from 60.99% to 96.24%. This may be due to the increases of the surface active sites of the electrode. However, when it was up to 20 times, the removal rate was decreased. The plot of $\ln(C_0/C_t)$ *vs.* t showed a line with the $R^2 \geq 0.978$, revealing that the degradation of CIP followed pseudo-first-order kinetics.[44] Then the degradation rate constants (k) were calculated (Table S3†). It could be seen that the SSO-16 had the highest k value of 0.0355 min^{-1}, which was consistent with the characterization of the electrodes (OEP = 2.2 V).

CIP could produce fluorescence due to the presence of conjugated heterocycles in its molecule.[45] In this study, 3D EEM was used to analyze the process of electrocatalytic degradation of CIP with the SSO-16 electrode. As shown in Fig. S3,† there were two fluorescent peaks at E_x/E_m = 250–300/400–500 nm and E_x/E_m = 300–350/400–500 nm in the initial CIP solution.[46] The fluorescence intensity of the two peaks gradually decreased, possibly due to the destruction of the conjugated heterocyclic structure of CIP or its intermediate product.[35] When the degradation time reached 90 minutes, no peak was observed, which proved that CIP could be effectively degraded by the SSO-16 electrode. Therefore, the SSO-16 electrode was selected.

3.3.2. Effect of current density. The effect of current density on the removal of CIP was shown in Fig. 4a, CIP degradation followed pseudo-first-order kinetics. The k values significantly

increased from 0.0232 to 0.0682 min^{-1} with the current density increasing from 10 to 25 mA cm^{-2} (Table S3†), which indicated that current density was a key experimental parameter affecting the electrocatalytic degradation process. Because it was closely related to the formation of hydroxyl radicals on the surface of the electrode.[13] With the increase of current density, more hydroxyl radicals would be formed on the electrode surface, thus increasing the removal efficiency and k value.[47]

The CVs of SSO-16 in 0.1 M Na_2SO_4 solution with the absence and presence of 30 mg L^{-1} CIP were conducted and the results were shown in Fig. S4.† When 30 mg L^{-1} CIP was added into the supporting electrolyte, there was no additional peak, suggesting that no direct electron exchange existed between CIP and the electrode, and the indirect oxidation should account for the majority of the reaction.[48] The results of fluorescence detection (Fig. S5†) demonstrated the formation of hydroxyl radicals during electrolysis. Thus, it could be deduced reasonably that the removal of CIP was mainly due to the oxidation of hydroxyl radicals. However, it was reported that the higher current density meant the higher energy consumption, more annoying

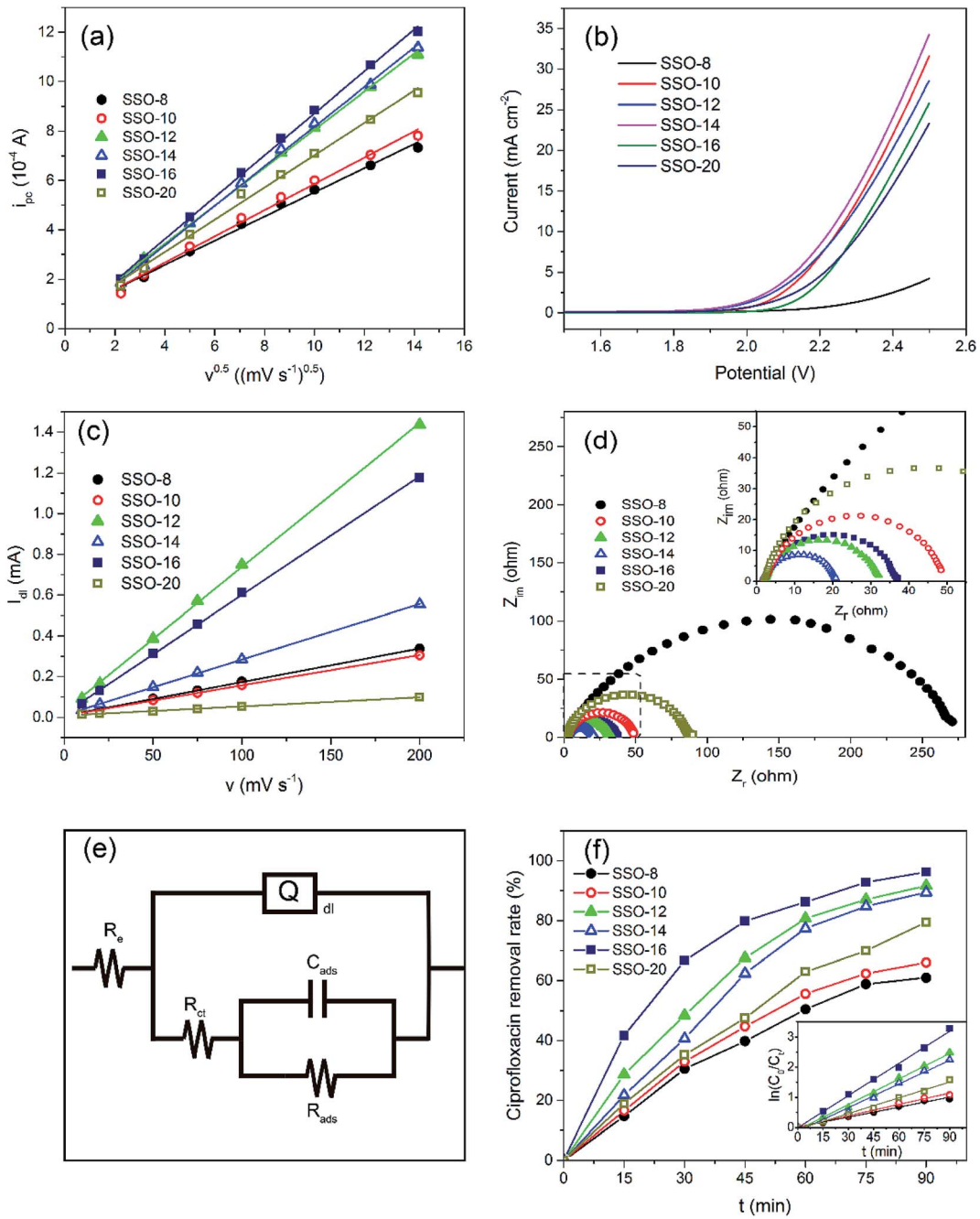

Fig. 3 Electrochemical performance of the prepared electrodes: (a) CV peak current i_{pc} in 1 mM $K_3Fe(CN)_6$ solution, (b) LSV curves in 0.5 M H_2SO_4 solution at a scan rate of 50 mV s^{-1}, (c) I_{dl} of CVs in 0.5 M KOH solution, (d) Nyquist plots of the different electrodes and (e) equivalent circuit model, (f) CIP removal (current density = 15 mA cm^{-2}, Na_2SO_4 concentration = 20 g L^{-1}, initial CIP concentration = 30 mg L^{-1}, and initial pH = 5). Inset shows the kinetic analysis for CIP removal assuming a pseudo-first-order kinetics.

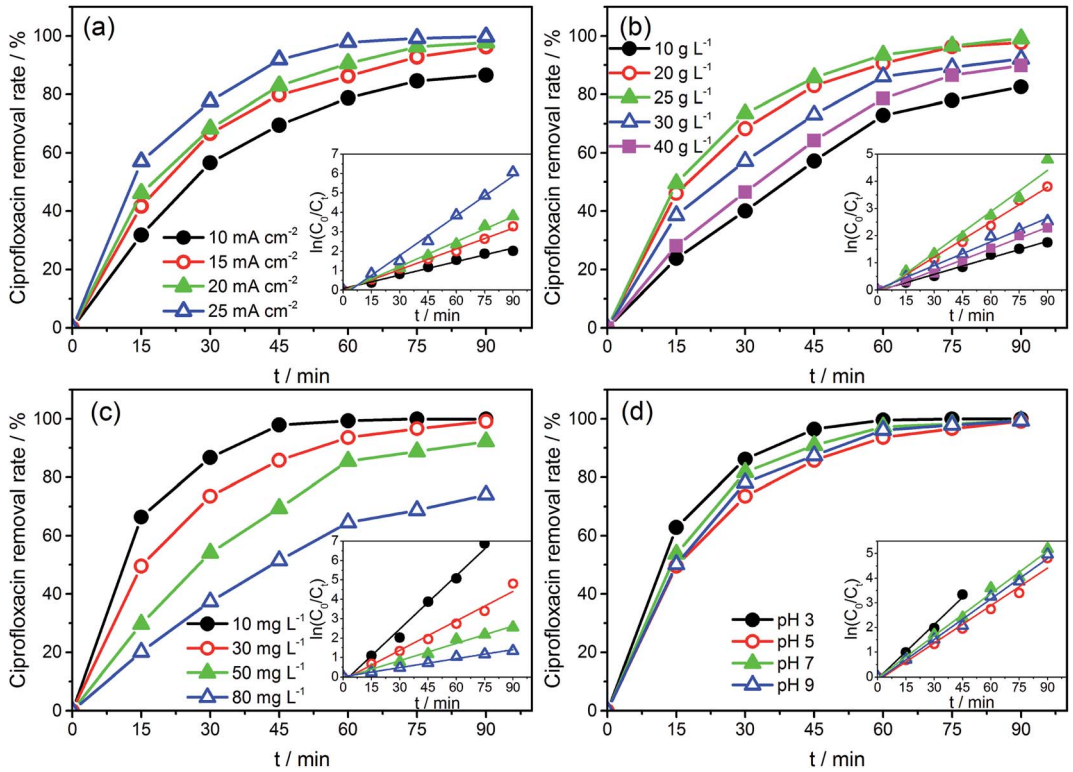

Fig. 4 The removal rates of CIP with (a) different current densities (Na_2SO_4 concentration = 25 g L^{-1}, initial CIP concentration = 30 mg L^{-1}, and initial pH = 5), (b) different electrolyte concentrations (current density = 20 mA cm^{-2}, initial CIP concentration = 30 mg L^{-1}, and initial pH = 5), (c) different initial concentrations (current density = 20 mA cm^{-2}, Na_2SO_4 concentration = 25 g L^{-1}, and initial pH = 5), and (d) different pH value (current density = 20 mA cm^{-2}, Na_2SO_4 concentration = 25 g L^{-1}, and initial CIP concentration = 30 mg L^{-1}). Inset shows kinetic analysis for CIP removal assuming a pseudo-first-order kinetics.

oxygen evolution, and shorter lifetime of the electrode.[49] Correspondingly, 20 mA cm^{-2} was selected for the subsequent degradation experiment.

3.3.3. Effect of electrolyte concentration. The effect of electrolyte concentration (ranging from 10 to 40 g L^{-1}) was shown in Fig. 4b and Table S3.† With the increase of the electrolyte concentration, the removal rates and k values increased to the peak at 25 g L^{-1} gradually and then decreased. It was due to that the concentration of electrolyte would affect the charge transfer process of the solution. As the electrolyte concentration increasing, the conductivity of the solution increased and the charge transferred faster, which was favorable to the degradation of organics. In addition, SO_4^{2-} from the electrolyte would lose more electrons to form another strong oxidant, $S_2O_8^{2-}$.[39] However, when the electrolyte concentration was higher, more SO_4^{2-} ions were absorbed on the electrode surface and consume hydroxyl radicals, which was not conducive to the formation of hydroxyl radicals and the degradation of organics.[50,51] Hence, 25 g L^{-1} of Na_2SO_4 was selected for further studies.

3.3.4. Effect of initial CIP concentration. The effect of the initial concentration of CIP on the electrocatalytic degradation was examined. The results (in Fig. 4c and Table S3†) showed that the degradation rate and k values decreased gradually with the increase of the initial concentration of CIP. When the CIP concentration was 10 mg L^{-1}, it could be completely removed within 30 min, but when the concentration was 80 mg L^{-1}, only 70% was removed even in 90 min. The k values also decreased from 0.144 to 0.013 min^{-1}. This results were in accord with the reports in the literatures.[39,51] The generated hydroxyl radicals

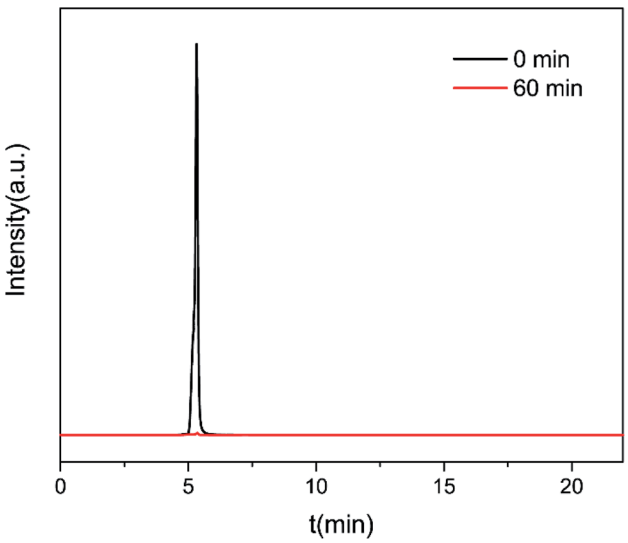

Fig. 5 Typical chromatograms of CIP solution at 0 min and 60 min under the optimized electrocatalytic degradation conditions (current density = 20 mA cm^{-2}, Na_2SO_4 concentration = 25 g L^{-1}, initial CIP concentration = 30 mg L^{-1}, and initial pH = 5).

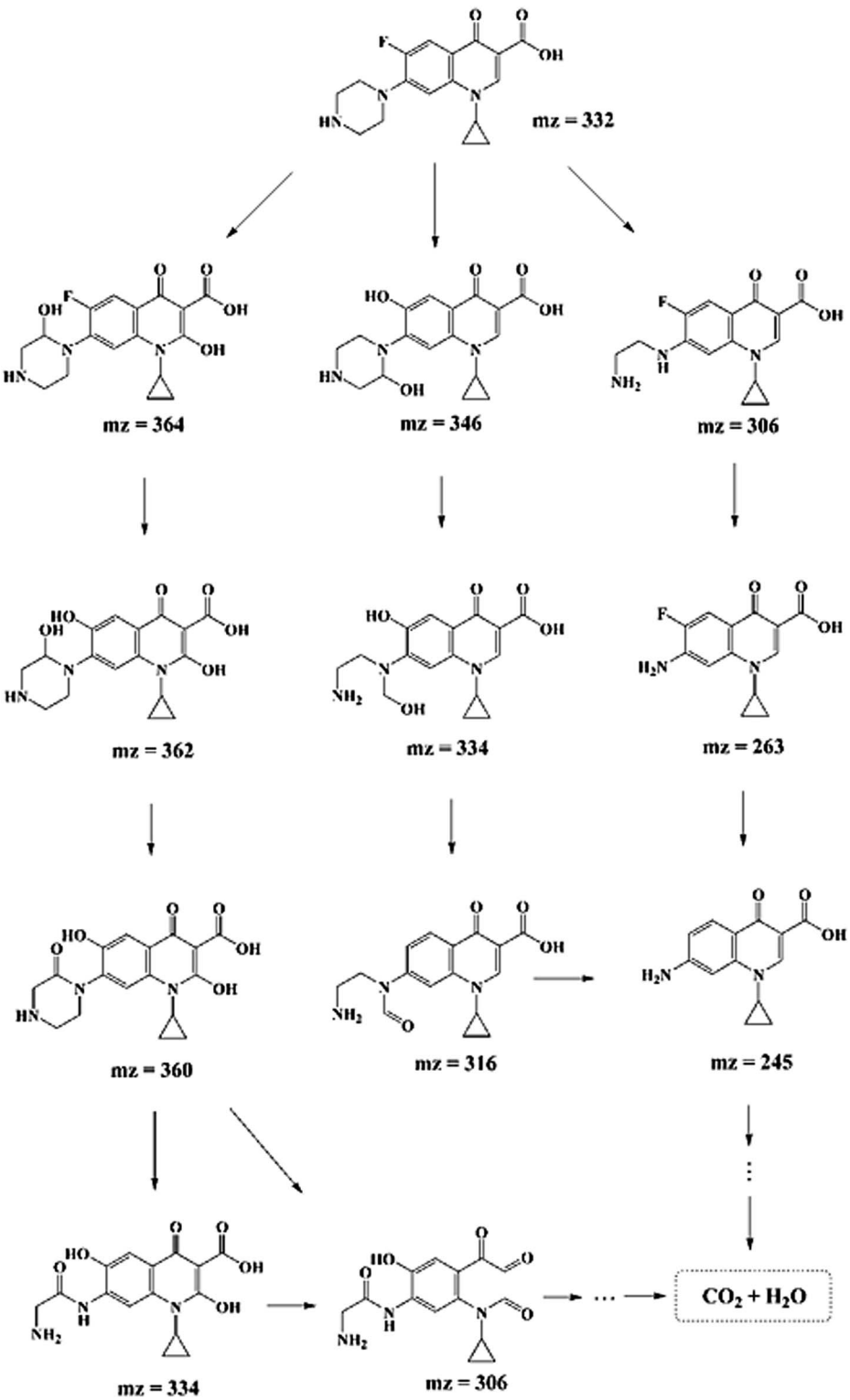

Scheme 1 Possible degradation pathways for CIP degradation with SSO-16 electrode.

was constant under a constant current condition.[52] When the initial concentration is low, the higher ratio of hydroxyl radicals to CIP would guarantee that the CIP molecules could be attacked by hydroxyl radicals effectively. However, when the initial concentration is high, it would take a longer time to produce enough hydroxyl radicals for attacking large numbers of CIP molecules. Also with the increase of concentration, more intermediates would be produced and accumulated on the surface of anode, leading to a contaminated surface and weakened electro-oxidation rates.[39] In view of the utilization of

the generated hydroxyl radicals, a moderate concentration of 30 mg L^{-1} was applied for the follow-up experiments.

3.3.5. Effect of initial pH value. The original pH of the CIP in solution was around 5, and the pH was adjusted by 0.5 M H_2SO_4 or NaOH. As shown in Fig. 4d and Table S3,† the removal of CIP was the fastest when pH was 3, and CIP could be almost completely removed within 60 min, while the removal rate was the lowest at pH 5. The results suggested that the solution pH was an important factor affecting the electrochemical process. Generally, the OEP of the electrode in the acidic system was relatively higher, thus, the oxygen evolution was more difficult to occur, and more hydroxyl radicals would be generated to react with the CIP molecules. At the same time, it should be mentioned that the amphiphilic compound CIP was negatively charged in neutral and alkaline systems, and positively charged in acidic systems, correspondingly the molecules were apt to be driven by the electric field and diffused to the anode region in neutral and alkaline systems to meet with hydroxyl radical, which would benefit the reaction and thus caused a relative high removal rate with pHs of 7 and 9.[53,54]

Under the optimized operation conditions (*i.e.*, current density of 20 mA cm^{-2}, Na_2SO_4 concentration of 25 g L^{-1}, and initial pH of 3.0), the removal rate of 30 mg L^{-1} CIP solution (100 mL) could reach to almost 100% with the SSO-16 electrode within 60 min, which was confirmed by the representative chromatograms of the CIP solution obtained by HPLC-MS/MS (Fig. 5). The TOC removal rate was displayed in Fig. S6,† and it could reach to 93% within 90 min, implying that the mineralization of the target would take longer. It may be related to the removal of the intermediates.

3.4. Analysis of the degradation pathway of CIP

In order to explore the degradation mechanism of CIP in this system, HPLC-MS/MS was used to identify the main intermediates in the degradation process. The peak areas of those intermediates changed with time (shown in Fig. S7†). In addition, based on the molecular structure of CIP, mass spectrometry information of intermediates and characteristic fragment ions, the structure of intermediates was reasonably inferred (listed in Table S4†). And according to previous studies,[11,35,55] the possible degradation pathways of CIP were proposed, as shown in Scheme 1, which mainly included the removal of fluorine and the destruction of piperazine ring of quinolones. The three degradation pathways were staggered, and gradually achieved the goal of degrading CIP into small molecules.

3.5. Reusability

In order to evaluate the reusability of the electrodes, eight cycles of experiments were performed using the SSO-16 electrode under the optimized electrocatalytic conditions. As shown in Fig. 6, the removal rate of CIP could remain almost 100% with the electrode used 7 times. The removal rate had a slight decrease (94.27%) in the eighth reuse of the electrode. As seen in Fig. S8 and S9,† the particles on the surface of the SSO-16 electrode after the eighth reuse were broken slightly, while its XRD pattern had no obvious change. It indicated that the electrode was stable and reusable.

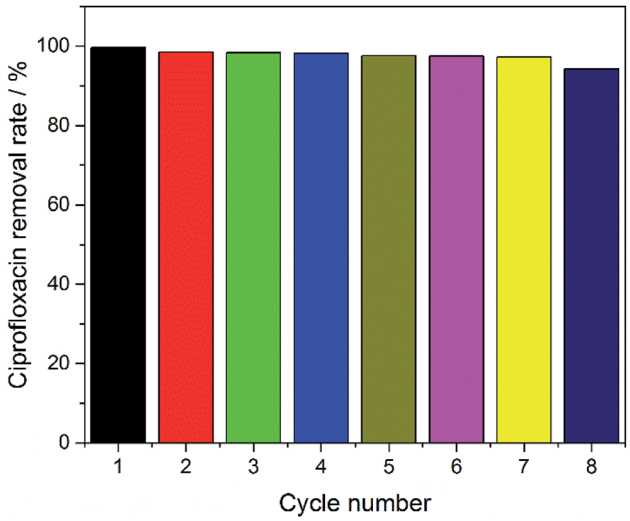

Fig. 6 Removal rates of CIP in cycle experiments with SSO-16 electrode.

4. Conclusion

SSO electrodes were successfully prepared by the sol–gel method. The coating times were found to have a remarkable influence on the electrocatalytic activity of the electrodes, and 12 to 16 times were the preferred coating times. The SSO-16 electrode with the highest OEP of 2.2 V exhibited excellent electrocatalytic degradation ability on CIP and reusability. Fluorescence spectroscopy and CV demonstrated that there were hydroxyl radicals produced during the degradation process and that CIP degradation was mainly from the attack of the hydroxyl radicals. Degradation experiments showed that the SSO-16 could remove CIP completely in 60 min with an initial concentration of 30 mg L^{-1} under the conditions: current density of 20 mA cm^{-2}, Na_2SO_4 concentration of 25 g L^{-1} and initial pH value of 3. Based on the results of HPLC-MS/MS, the possible CIP degradation pathway was proposed.

Conflicts of interest

The authors declare no competing financial interest.

Acknowledgements

This work was supported by the National Special Fund for Agro-scientific Research in the Public Interest of China (No. 201503108) and Science & Technology Project of Hunan Province (No. 2017WK2091).

References

1 Q. Bu, B. Wang, J. Huang, K. Liu, S. Deng, Y. Wang and G. Yu, *Chemosphere*, 2016, **144**, 1384–1390.

2 M. Zhang, Y. Shi, Y. Lu, A. C. Johnson, S. Sarvajayakesavalu, Z. Liu, C. Su, Y. Zhang, M. D. Juergens and X. Jin, *Sci. Total Environ.*, 2017, **590**, 633–642.
3 E. M. Golet, A. C. Alder and W. Giger, *Environ. Sci. Technol.*, 2002, **36**, 3645–3651.
4 E. M. Golet, A. Strehler, A. C. Alder and W. Giger, *Anal. Chem.*, 2002, **74**, 5455–5462.
5 H. Lin, H. Li, L. Chen, L. Li, L. Yin, H. Lee and Z. Yang, *Ecotoxicol. Environ. Saf.*, 2018, **147**, 530–536.
6 V. N. Binh, N. Dang, N. T. K. Anh, L. X. Ky and P. K. Thai, *Chemosphere*, 2018, **197**, 438–450.
7 C. X. Yan, Y. Yang, J. L. Zhou, M. Liu, M. H. Nie, H. Shi and L. J. Gu, *Environ. Pollut.*, 2013, **175**, 22–29.
8 R. Mirzaei, M. Yunesian, S. Nasseri, M. Gholami, E. Jalilzadeh, S. Shoeibi and A. Mesdaghinia, *Sci. Total Environ.*, 2018, **619–620**, 446–459.
9 M. B. Ahmed, J. L. Zhou, H. H. Ngo and W. S. Guo, *Sci. Total Environ.*, 2015, **532**, 112–126.
10 J. R. Chen, F. X. Qiu, W. Z. Xu, S. S. Cao and H. J. Zhu, *Appl. Catal., A*, 2015, **495**, 131–140.
11 X. Y. Zheng, S. P. Xu, Y. Wang, X. Sun, Y. Gao and B. Y. Gao, *J. Colloid Interface Sci.*, 2018, **527**, 202–213.
12 B. Tang, J. N. Du, Q. M. Feng, J. Q. Zhang, D. Wu, X. K. Jiang, Y. Dai and J. L. Zou, *J. Colloid Interface Sci.*, 2018, **517**, 28–39.
13 J. Chen, Y. Xia and Q. Dai, *Electrochim. Acta*, 2015, **165**, 277–287.
14 M. Zhu, C. Zhai, M. Sun, Y. Hu, B. Yan and Y. Du, *Appl. Catal., B*, 2017, **203**, 108–115.
15 J. Hu, C. Zhai, H. Gao, L. Zeng, Y. Du and M. Zhu, *Sustainable Energy and Fuels*, 2019, **3**, 439–449.
16 C. Zhai, M. Sun, L. Zeng, M. Xue, J. Pan, Y. Du and M. Zhu, *Appl. Catal., B*, 2019, **243**, 283–293.
17 T. Velegraki, G. Balayiannis, E. Diamadopoulos, A. Katsaounis and D. Mantzavinos, *Chem. Eng. J.*, 2010, **160**, 538–548.
18 I. Sires, E. Brillas, G. Cerisola and M. Panizza, *J. Electroanal. Chem.*, 2008, **613**, 151–159.
19 J. Lv, Y. Feng, J. Liu, Y. Qu and F. Cui, *Appl. Surf. Sci.*, 2013, **283**, 900–905.
20 Y. Yao, L. Jiao, N. Yu, F. Guo and X. Chen, *J. Solid State Electrochem.*, 2016, **20**, 353–359.
21 J. Mora-Gomez, E. Ortega, S. Mestre, V. Perez-Herranz and M. Garcia-Gabaldon, *Sep. Purif. Technol.*, 2019, **208**, 68–75.
22 L. Yu, Y. Chen, W. Han, X. Sun, J. Li and L. Wang, *RSC Adv.*, 2016, **6**, 19848–19856.
23 M. Seo, Y. Akutsu and H. Kagemoto, *Ceram. Int.*, 2007, **33**, 625–629.
24 M. E. Makgae, M. J. Klink and A. M. Crouch, *Appl. Catal., B*, 2008, **84**, 659–666.
25 H. M. Bai, P. He, J. C. Chen, K. L. Liu, H. Lei, X. J. Zhang, F. Q. Dong and H. Li, *Water Sci. Technol.*, 2017, **75**, 220–227.
26 H. Y. Ding, Y. J. Feng and J. F. Liu, *Mater. Lett.*, 2007, **61**, 4920–4923.
27 A. N. S. Rao, V. T. Venkatarangaiah, G. B. Nagarajappa, S. H. Nataraj and P. M. Krishnegowda, *J. Environ. Chem. Eng.*, 2017, **5**, 4969–4979.
28 P. D. Yao, Q. N. Jin, X. M. Chen, Y. Q. Xing and D. H. Wang, *Electrochem. Solid-State Lett.*, 2008, **11**, J37–J39.
29 A. S. Huang, G. H. Zhao and H. X. Li, *Chin. Chem. Lett.*, 2007, **18**, 997–1000.
30 X. Lei, L. Li, Y. Chen and Y. Hu, *Environ. Sci. Pollut. Res.*, 2018, **25**, 11683–11693.
31 C. M. Fan, B. Hua, Y. Wang, Z. H. Liang, X. G. Hao, S. B. Liu and Y. P. Sun, *Desalination*, 2009, **249**, 736–741.
32 Z. R. Sun, H. Zhang, X. F. Wei, R. Du and X. Hu, *J. Electrochem. Soc.*, 2015, **162**, H590–H596.
33 H. Ding, Y. Feng, J. Lue and J. Liu, *Chin. J. Anal. Chem.*, 2007, **35**, 1395–1399.
34 A. M. El-Kosasy, O. Abdel-Aziz, N. Magdy and N. M. El Zahar, *Spectrochim. Acta, Part A*, 2016, **157**, 26–33.
35 X. J. Wen, C. G. Niu, L. Zhang, C. Liang, H. Guo and G.-M. Zeng, *J. Catal.*, 2018, **358**, 141–154.
36 Y. Duan, Y. Chen, Q. Wen and T. Duan, *J. Electroanal. Chem.*, 2016, **768**, 81–88.
37 T. G. Duan, Y. Chen, Q. Wen and Y. Duan, *RSC Adv.*, 2015, **5**, 19601–19612.
38 L. Li, Z. Huang, X. Fan, Z. Zhang, R. Dou, S. Wen, Y. Chen, Y. Chen and Y. Hu, *Electrochim. Acta*, 2017, **231**, 354–362.
39 P. Z. Duan, X. Hu, Z. Y. Ji, X. M. Yang and Z. R. Sun, *Chemosphere*, 2018, **212**, 594–603.
40 M. J. Gira, K. P. Tkacz and J. R. Hampton, *Nano convergence*, 2016, **3**, 6.
41 R. Mei, Q. Wei, C. Zhu, W. Ye, B. Zhou, L. Ma, Z. Yu and K. Zhou, *Appl. Catal., B*, 2019, **245**, 420–427.
42 S. Ferro, D. Rosestolato, C. A. Martínez-Huitle and A. De Battisti, *Electrochim. Acta*, 2014, **146**, 257–261.
43 A. Oury, A. Kirchev and Y. Bultel, *Electrochim. Acta*, 2012, **63**, 28–36.
44 Y. Wang, C. Shen, M. Zhang, B.-T. Zhang and Y.-G. Yu, *Chem. Eng. J.*, 2016, **296**, 79–89.
45 S. N. Yin, T. Yao, T.-H. Wu, Y. Zhang and P. Wang, *Talanta*, 2017, **174**, 14–20.
46 X. J. Wen, C.-G. Niu, L. Zhang, C. Liang and G.-M. Zeng, *Appl. Catal., B*, 2018, **221**, 701–714.
47 L. Feng, E. D. van Hullebusch, M. A. Rodrigo, G. Esposito and M. A. Oturan, *Chem. Eng. J.*, 2013, **228**, 944–964.
48 H. An, H. Cui, W. Zhang, J. Zhai, Y. Qian, X. Xie and Q. Li, *Chem. Eng. J.*, 2012, **209**, 86–93.
49 D. Shao, J. Liang, X. Cui, H. Xu and W. Yan, *Chem. Eng. J.*, 2014, **244**, 288–295.
50 H. Alemu and L. Hlalele, *Bull. Chem. Soc. Ethiop.*, 2007, **21**, 1–12.
51 J. Wang, L. Tang, G. Zeng, Y. Deng, Y. Liu, L. Wang, Y. Zhou, Z. Guo, J. Wang and C. Zhang, *Appl. Catal., B*, 2017, **209**, 285–294.
52 C. A. Martínez-Huitle and E. Brillas, *Appl. Catal., B*, 2009, **87**, 105–145.
53 L. Ge, J. Chen, X. Wei, S. Zhang, X. Qiao, X. Cai and Q. Xie, *Environ. Sci. Technol.*, 2010, **44**, 2400–2405.
54 X. Yu, G. L. Zipp and G. W. R. Davidson Iii, *Pharm. Res.*, 1994, **11**, 522–527.
55 T. An, H. Yang, G. Li, W. Song, W. J. Cooper and X. Nie, *Appl. Catal., B*, 2010, **94**, 288–294.